JPEDAV (2013) 34:438–446
DOI: 10.1007/s11669-013-0257-7
1547-7037 ©ASM International

Experimental Investigation of Phase Equilibria in the Cu-Fe-Zr Ternary System

W.L. Huang, Y. Yu, S.Y. Yang, C.P. Wang, X.J. Liu, R. Kainuma, and K. Ishida

(Submitted November 29, 2012; in revised form June 14, 2013; published online July 26, 2013)

The phase equilibria in the Cu-Fe-Zr ternary system was experimentally investigated by optical microscopy, electron probe micro-analyzer and x-ray diffraction on the equilibriated alloys. Three isothermal sections of the Cu-Fe-Zr ternary system at 1000, 1100 and 1200 °C were experimentally determined, and no ternary compound was found in this system. The further result in the present work shows that the $Fe_{23}Zr_6$ phase in the Cu-Fe-Zr ternary system is an equilibrium phase rather than oxygen-stabilized phase.

Keywords Cu-Fe-Zr ternary system, electron probe micro-analyzer, experimental phase equilibria, x-ray diffraction

1. Introduction

Metallic glasses have stimulated widespread research enthusiasm due to its excellent properties of strength, hardness, magnetism, wear and corrosion resistance.[1-3] However, the applications of metallic glasses have been limited due to the poor plasticity caused by shear localization and work softening.[4] To solve this problem, great attention has been paid to crystalline/amorphous composite through liquid immiscibility.[5-7] The Cu-Fe-Zr-B is a good candidate for the composites, owing to its sufficiently high glass-forming ability (GFA) in the Fe-Zr-B system,[8] and a positive enthalpy of mixing in the Fe-Cu atomic pair.[9] The phase equilibria information in the Cu-Fe-Zr ternary subsystem is needed to pinpoint the alloy compositions with liquid immiscibility in the Cu-Fe-Zr-B quaternary system. However, until now, such information in the Cu-Fe-Zr ternary system has not been available in the relevant literature. Therefore, it is necessary to comprehensively determine the phase equilibria in the Cu-Fe-Zr ternary system.

Three binary phase diagrams of the Cu-Fe,[10] Cu-Zr[11] and Fe-Zr,[12] constituting the Cu-Fe-Zr ternary system, are shown in Fig. 1. The Cu-Fe binary system[10] is a simple system without any intermediate phase. The Cu-Zr binary system[11] has ten intermediate phases, Cu_5Zr, $Cu_{51}Zr_{14}$, Cu_8Zr_3, Cu_2Zr, $Cu_{24}Zr_{13}$, $Cu_{10}Zr_7$, CuZr, Cu_5Zr_8, $\alpha CuZr_2$ and $\beta CuZr_2$. The Cu_5Zr phase forms through peritectic reaction at 1012 °C. The Fe-Zr binary system[12] has five intermediate phases, $FeZr_3$, $FeZr_2$, αFe_2Zr, βFe_2Zr and $Fe_{23}Zr_6$. All the stable solid phases in the three binary systems are summarized in Table 1.

The purpose of the present work is to experimentally investigate the phase equilibrium the Cu-Fe-Zr ternary system at 1000, 1100 and 1200 °C by using optical microscopy (OM), electron probe micro-analyzer (EPMA) and x-ray diffraction (XRD), which will provide a better understanding of microstructures and information for the thermodynamic database of Cu-Fe-Zr-B quaternary phase diagram.

2. Experimental Procedure

Highly-pure copper (99.9 wt.%), iron (99.9 wt.%) and zirconium (99.9 wt.%) were used as starting materials. Bulk alloy buttons were prepared from pure elements by arc melting under a highly-pure argon atmosphere using a non-consumable tungsten electrode. The ingots were melted at least five times in order to achieve their homogeneity. The sample weight was around 10 g and the weight loss during melting was generally less than 0.20%. Afterwards, the ingots were cut into small pieces for heat treatment and further observations.

All samples were put into quartz capsules evacuated and backfilled with argon gas. The specimens were annealed at 1000, 1100 and 1200 °C, respectively. The time of heat treatment varied from several hours to several days depending on the annealing temperature and the composition of the specimen. After the heat treatment, the specimens were quenched into ice water.

After annealing standard metallographic preparation, the microstructural observations were carried out by OM. The equilibrium compositions of the phases were measured by EPMA (JXA-8800R, JEOL, Japan). Pure elements were used as standards and measurements were carried out at 20.0 kV. The XRD was used to identify the crystal structure of the constituent phases. The XRD measurement was

W.L. Huang, Y. Yu, S.Y. Yang, C.P. Wang, and **X.J. Liu,** Department of Materials Science and Engineering, College of Materials, and Research Center of Materials Design and Applications, Xiamen University, Xiamen 361005, People's Republic of China; and **R. Kainuma** and **K. Ishida,** Department of Materials Science, Graduate School of Engineering, Tohoku University, Aoba-yama 6-6-02, Sendai 980-8579, Japan. Contact e-mail: lxj@xmu.edu.cn.

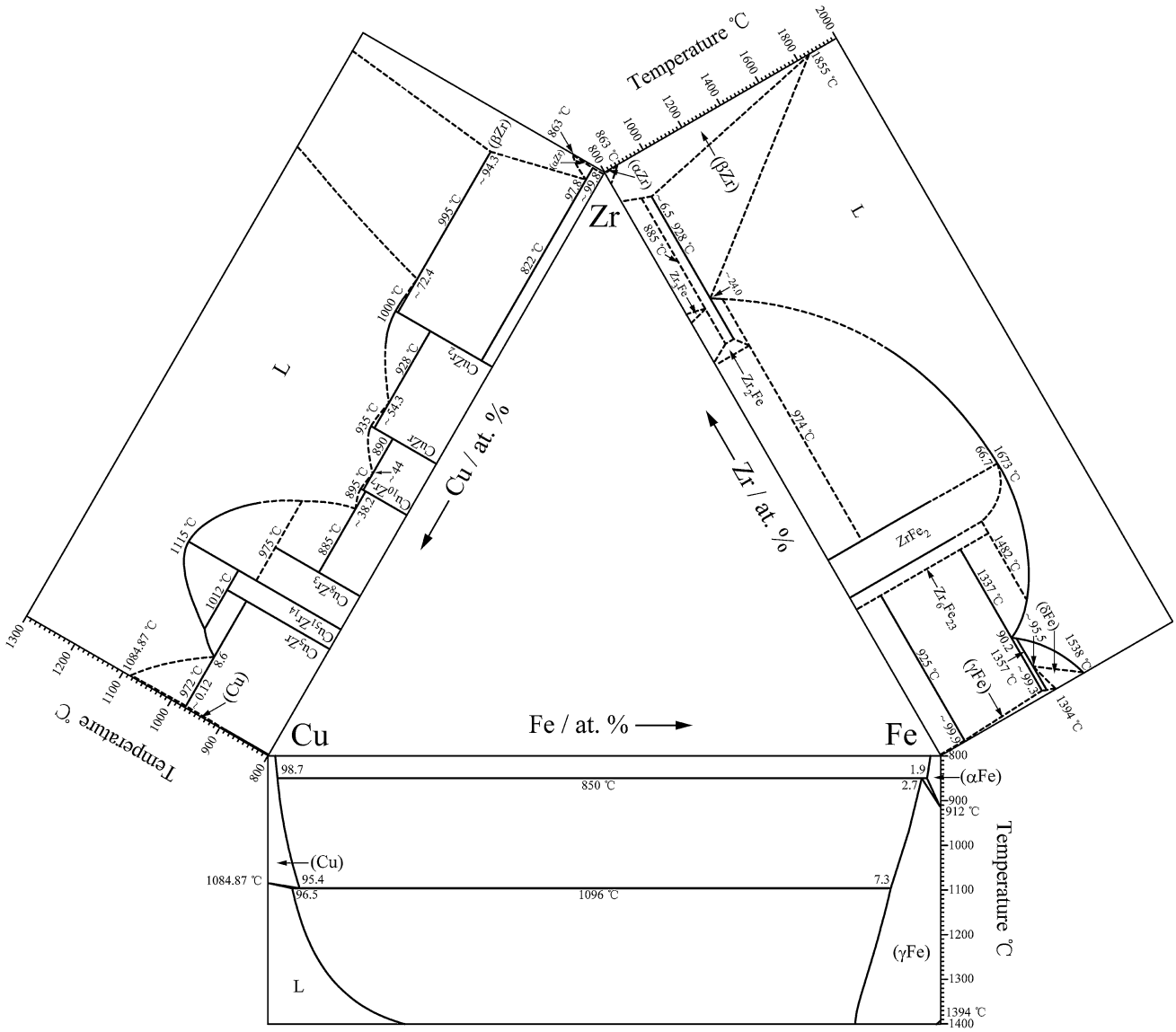

Fig. 1 Binary phase diagrams constituting the Cu-Fe-Zr ternary system[10-12]

carried out on a Bruker D8 Advance X-pert diffractometer using CuK_α radiation at 35.0 kV and 20 mA. The data were collected in the range of 2θ from 20° to 120° at a step of 0.02°.

3. Results and Discussion

3.1 Microstructure and Phase Equilibria

Back-scattered electron (BSE) images of typical ternary Cu-Fe-Zr alloys are shown in Fig. 2(a)-(j). Phase identification was based on the equilibrium composition measured by EPMA and XRD results. Figure 2(a) shows the two-phase microstructure ((αFe) + Liquid) of the $Cu_{49.5}Fe_{49.5}Zr_1$ (at.%) alloy annealed at 1200 °C for 1 day. In the $Cu_5Fe_{85}Zr_{10}$ (at.%) alloy annealed at 1100 °C for 60 days, the two-phase microstructure ($Fe_{23}Zr_6$ + (αFe)) was observed (Fig. 2b) and substantiated by the XRD result, as shown in Fig. 3(a), where the characteristic peaks of the $Fe_{23}Zr_6$ and (αFe) phases were found and well marked by different symbols. The (αFe) phase at room temperature came from the phase transition in (γFe) phase during quenching. Moreover, the composition of the (αFe) phase at room temperature and the (γFe) phase at high temperature are the same. The oxygen-content detected by EPMA in the $Fe_{23}Zr_6$ phase in all samples is very low in the Cu-Fe-Zr ternary system, which is different from the $Fe_{23}Zr_6$ phase stabilized by oxygen in the Fe-Zr system.[26] Combined with the EPMA element mapping (Fig. 4) of the selected area of the $Cu_5Fe_{85}Zr_{10}$ (at.%) alloy annealed at 1100 °C for 60 days, the $Fe_{23}Zr_6$ phase is an equilibrium phase in the Cu-Fe-Zr ternary system.

Table 1 The stable solid phases in the three binary systems

System	Phase	Pearson's symbol	Prototype	Space group	Lattice parameters, nm	References
Cu-Fe	(Cu)	cF4	Cu	*Fm*-3*m*	a = 0.3613	[10,13]
	(δFe)	cI2	W	*Im*-3*m*	a = 0.29315	[10,14]
	(γFe)	cF4	Cu	*Fm*-3*m*	a = 0.343	[10,15]
	(αFe)	cI2	W	*Im*-3*m*	a = 0.2866	[10,14]
Cu-Zr	(Cu)	cF4	Cu	*Fm*-3*m*	a = 0.3613	[11,13]
	Cu_5Zr	cF24	$AuBe_5$	*F*-43*m*	a = 0.687	[11,16]
	$Cu_{51}Zr_{14}$	hP65	$Ag_{51}Gd_{14}$	*P*6/*m*	a = 1.12444, c = 0.82815	[11,17]
	Cu_8Zr_3	oP44	Cu_8Hf_3	*Pnma*	a = 0.78693, b = 0.81547, c = 0.99848	[11,17]
	Cu_2Zr	…	…	…	…	[11]
	$Cu_{24}Zr_{13}$	o*37	…	…	…	[11]
	$Cu_{10}Zr_7$	oC68	$Ni_{10}Zr_7$	*C*2*ca*	a = 1.26729, b = 0.93163, c = 0.93466	[11,17]
	CuZr	cP2	CsCl	*Pm*-3*m*	a = 0.32620	[11,18]
	Cu_5Zr_8	o*26	…	…	…	[11]
	β$CuZr_2$	tI6	$MoSi_2$	*I*4/*mmm*	a = 0.32204, c = 1.11832	[11,19]
	α$CuZr_2$	tP150	…	…	…	[11]
	(βZr)	cI2	W	*Im*-3 *m*	a = 0.3568	[11,20]
	(αZr)	hP2	Mg	$P6_3/mmc$	a = 0.3232, c = 0.5147	[11,21]
Fe-Zr	(δFe)	cI2	W	*Im*-3*m*	a = 0.29315	[12,14]
	(γFe)	cF4	Cu	*Fm*-3*m*	a = 0.343	[12,15]
	(αFe)	cI2	W	*Im*-3*m*	a = 0.2866	[12,14]
	$Fe_{23}Zr_6$	cF116	Th_6Mn_{23}	*Fm*-3*m*	a = 1.169	[12,22]
	βFe_2Zr	hP24	$MgNi_2$	$P6_3/mmc$	…	[12]
	αFe_2Zr	cF24	Cu_2Mg	*Fd*-3*m*	a = 0.70721	[12,23]
	$FeZr_2$	tI12	Al_2Cu	*I*4/*mcm*	a = 0.6385, c = 0,5596	[12,24]
	$FeZr_3$	oC16	BRe_3	*Cmcm*	a = 0.3324, b = 1.0990, c = 0.8810	[12,25]
	(βZr)	cI2	W	*Im*-3*m*	a = 0.3568	[12,20]
	(αZr)	hP2	Mg	$P6_3/mmc$	a = 0.3232, c = 0.5147	[12,21]

The $Cu_5Fe_{45}Zr_{50}$ (at.%) and $Cu_5Fe_{10}Zr_{85}$ (at.%) alloys annealed at 1100 °C are located in two two-phase equilibrium regions of the (Fe_2Zr + Liquid) and ((βZr) + Liquid), respectively, as characterized in Fig. 2(c) and (d). A three-phase equilibrium of the ($Fe_{23}Zr_6$ + (αFe) + (Cu)) was observed (Fig. 2e) in the $Cu_{49.5}Fe_{49.5}Zr_1$ (at.%) alloy annealed at 1000 °C for 60 days and the XRD results is shown in Fig. 3(b), where the characteristic peaks of $Fe_{23}Zr_6$, (αFe) and (Cu) phases were confirmed. Figure 2(f) presents the three-phase equilibrium microstructures of the ($Fe_{23}Zr_6$ + (αFe) + Liquid) in the $Cu_{45}Fe_{45}Zr_{10}$ (at.%) alloy annealed at 1200 °C for 2 days, and Fig. 2(g) shows a three-phase equilibrium of the ($Fe_{23}Zr_6$ + Fe_2Zr + Liquid) in the $Cu_{38}Fe_{38}Zr_{24}$ (at.%) alloy annealed at 1200 °C for 2 days. There is a three-phase equilibrium of the ($Fe_{23}Zr_6$ + Fe_2Zr + (Cu))in the $Cu_{41}Fe_{41}Zr_{18}$ (at.%) annealed at 1000 °C (Fig. 2h) and the XRD results is shown in Fig. 3(c). Two three-phase equilibria of the (Fe_2Zr + (Cu) + Liquid) and (Fe_2Zr + $Cu_{51}Zr_{14}$ + Liquid) were observed in the $Cu_{37}Fe_{37}Zr_{26}$ (at.%) and $Cu_{60}Fe_{10}Zr_{30}$ (at.%) alloys annealed at 1000 °C, and were indicated in Fig. 2(i) and (j), respectively. XRD results of the $Cu_{47.5}Fe_{47.5}Zr_5$ (at.%) and $Cu_5Fe_{85}Zr_{10}$ (at.%) alloys annealed at 1000 °C are presented in Fig. 3(d) and (e), respectively. According to the XRD results, the lattice parameters of phases in the $Cu_{49.5}Fe_{49.5}Zr_1$ (at.%), $Cu_{47.5}Fe_{47.5}Zr_5$ (at.%), $Cu_5Fe_{85}Zr_{10}$ (at.%), $Cu_{41}Fe_{41}Zr_{18}$ (at.%) alloys annealed at 1000 °C and $Cu_5Fe_{85}Zr_{10}$ (at.%) alloy annealed at 1100 °C have been calculated, respectively (Table 2).

3.2 Isothermal Section

The equilibrium compositions of the Cu-Fe-Zr ternary system at 1000, 1100 and 1200 °C obtained from EPMA are listed in Tables 3-5, respectively. Base on the experimental data determined by this work, three isothermal sections of 1000, 1100 and 1200 °C were constructed in Fig. 5(a)-(c), respectively.

Figure 5(a) shows the isothermal section at 1000 °C. In the section, four three-phase regions of ($Fe_{23}Zr_6$ + (γFe) + (Cu)), ($Fe_{23}Zr_6$ + Fe_2Zr + (Cu)), (Fe_2Zr + (Cu) + Liquid) and (Fe_2Zr + $Cu_{51}Zr_{14}$ + Liquid)) appear. The results show that the maximum solubility of Cu in the Fe_2Zr and $Fe_{23}Zr_6$ phases are about 15 and 5 at.%, respectively. In the isothermal section of 1100 °C shown in Fig. 5(b), two three-phase regions of ($Fe_{23}Zr_6$ + (γFe) + Liquid) and ($Fe_{23}Zr_6$ + Fe_2Zr + Liquid) were experimentally determined in this work. The maximum solubility of Cu in the Fe_2Zr phase was found to be about 12.5 at.%, and the maximum solubility of Cu in the $Fe_{23}Zr_6$ phase was approximately 4.5 at.%. The phase relationships in the isothermal section of 1200 °C

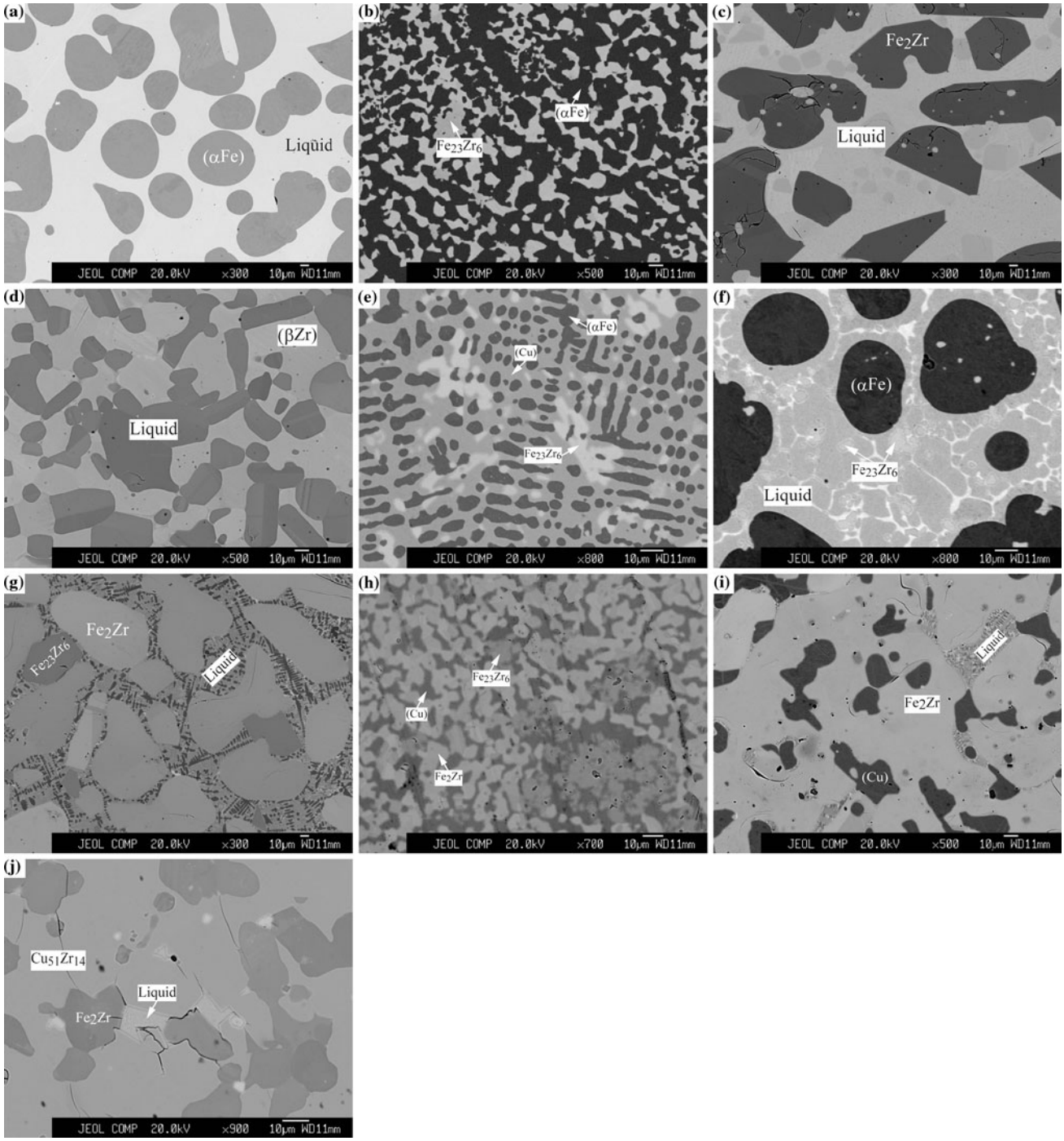

Fig. 2 Typical ternary BSE images obtained from: (a) $Cu_{49.5}Fe_{49.5}Zr_1$ (at.%) alloy annealed at 1200 °C for 1 day; (b) $Cu_5Fe_{85}Zr_{10}$ (at.%) alloy annealed at 1100 °C for 60 days; (c) $Cu_5Fe_{45}Zr_{50}$ (at.%) alloy annealed at 1100 °C for 4 days; (d) $Cu_5Fe_{10}Zr_{85}$ (at.%) alloy annealed at 1100 °C for 4 days; (e) $Cu_{49.5}Fe_{49.5}Zr_1$ (at.%) alloy annealed at 1000 °C for 60 days; (f) $Cu_{45}Fe_{45}Zr_{10}$ (at.%) alloy annealed at 1200 °C for 2 days; (g) $Cu_{38}Fe_{38}Zr_{24}$ (at.%) alloy annealed at 1200 °C for 2 days; (h) $Cu_{41}Fe_{41}Zr_{18}$ (at.%) alloy annealed at 1000 °C for 4 days; (i) $Cu_{37}Fe_{37}Zr_{26}$ (at.%) alloy annealed at 1000 °C for 4 days; and (j) $Cu_{60}Fe_{10}Zr_{30}$ (at.%) alloy annealed at 1000 °C for 12 h

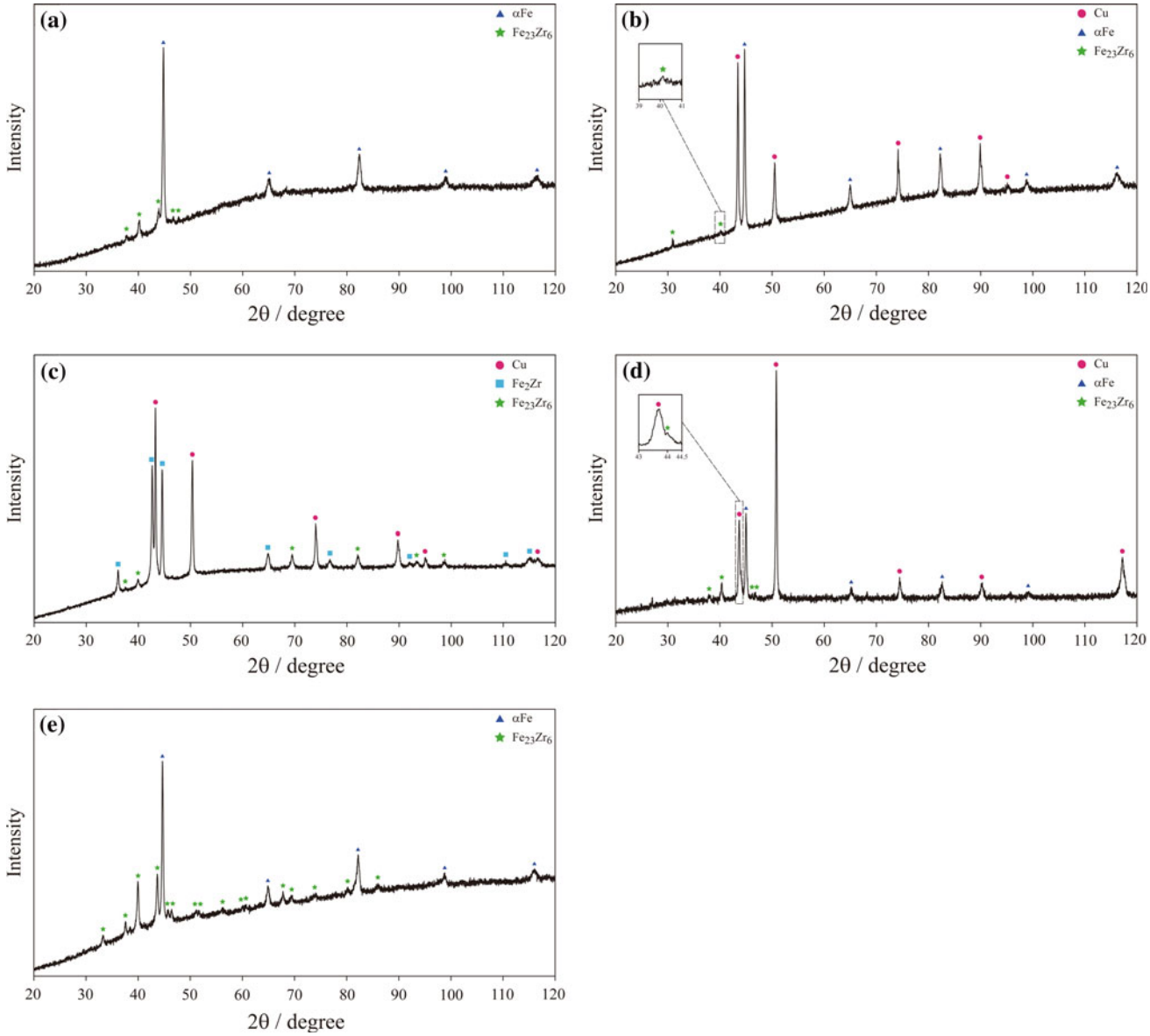

Fig. 3 X-ray diffraction patterns obtained from: (a) the $Cu_5Fe_{85}Zr_{10}$ (at.%) alloy annealed at 1100 °C for 60 days; (b) the $Cu_{49.5}Fe_{49.5}Zr_1$ (at.%) alloy annealed at 1000 °C for 60 days; (c) the $Cu_{41}Fe_{41}Zr_{18}$ (at.%) alloy annealed at 1000 °C for 4 days; (d) $Cu_{47.5}Fe_{47.5}Zr_5$ (at.%) alloy annealed at 1000 °C for 60 days; and (e) the $Cu_5Fe_{85}Zr_{10}$ (at.%) alloy annealed at 1000 °C for 60 days

containing two three-phase regions of ($Fe_{23}Zr_6$ + (γFe) + Liquid) and ($Fe_{23}Zr_6$ + Fe_2Zr + Liquid) (Fig. 5c), is quite similar to that at 1100 °C. Undetermined three-phase equilibria in Fig. 5(a) and (b) are shown in dashed lines. Compared with the above mentioned three isothermal sections, it should be noted that the area of liquid phase increases at the temperature range from 1000 to 1200 °C.

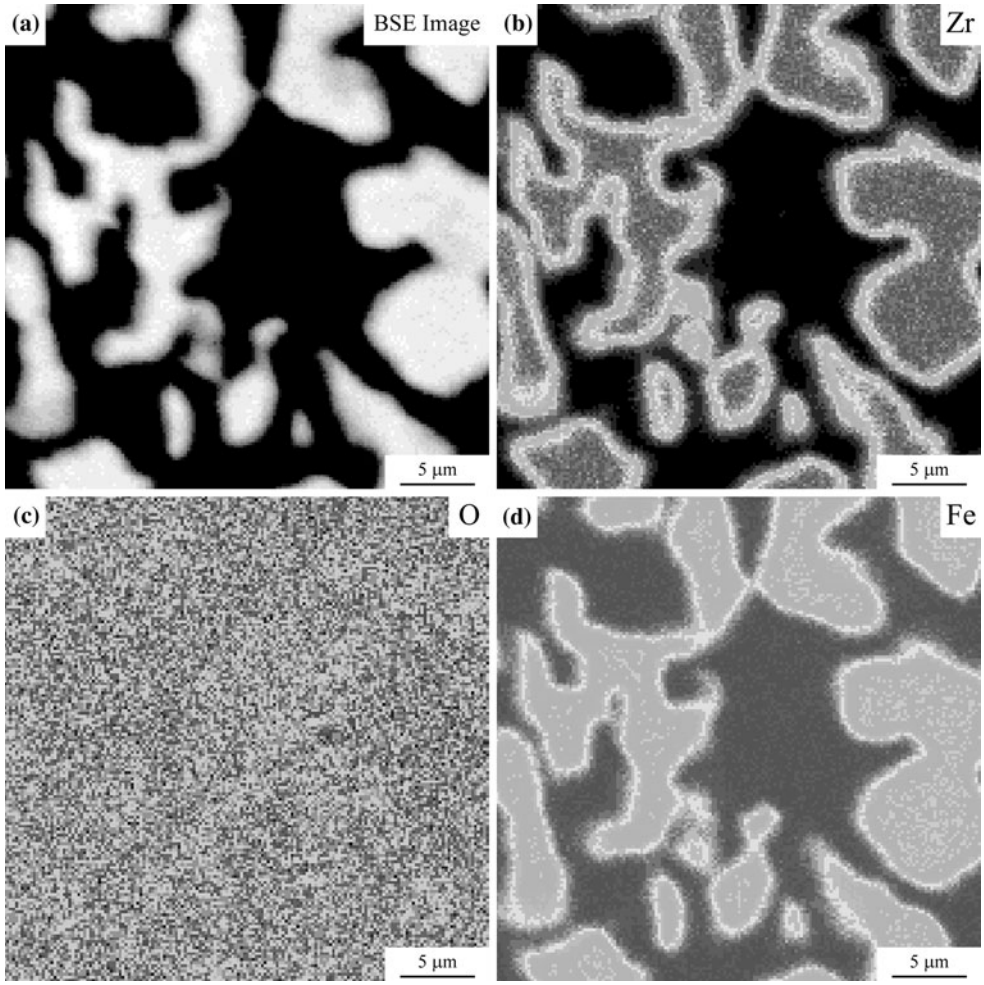

Fig. 4 $Fe_{23}Zr_6$-enriched region of the Cu5Fe85Zr10 (at.%) alloy annealed at 1100 °C for 60 days: (a) BSE micrograph of the region with (αFe) (dark areas), and $Fe_{23}Zr_6$ (white areas); (b, c, and d) EPMA element mappings of the respective region for zirconium, oxygen, and iron, respectively

Table 2 The calculating lattice parameters of phases in typical ternary Cu-Fe-Zr alloys

Alloys, at.%	Annealing temperature, °C	XRD pattern	Phase	Calculating lattice parameters, nm
$Cu_{49.5}Fe_{49.5}Zr_1$	1000	Figure 3(b)	(αFe)	a = 0.2870
			Fe23Zr6	a = 1.1659
			(Cu)	a = 0.3616
$Cu_{47.5}Fe_{47.5}Zr_5$	1000	Figure 3(d)	(αFe)	a = 0.2868
			Fe23Zr6	a = 1.1675
			(Cu)	a = 0.3618
$Cu_5Fe_{85}Zr_{10}$	1000	Figure 3(e)	(αFe)	a = 0.2871
			Fe23Zr6	a = 1.1713
$Cu_{41}Fe_{41}Zr_{18}$	1000	Figure 3(c)	Fe2Zr	a = 0.7037
			Fe23Zr6	a = 1.1668
			(Cu)	a = 0.3620
$Cu_5Fe_{85}Zr_{10}$	1100	Figure 3(a)	(αFe)	a = 0.2868
			Fe23Zr6	a = 1.1695

Table 3 Equilibrium compositions of the Cu-Fe-Zr system at 1000 °C

Alloys, at.%	Annealing time	Phase equilibria Phase 1/Phase 2/Phase 3	Composition, at.%								
			Phase 1			Phase 2			Phase 3		
			Cu	Fe	Zr	Cu	Fe	Zr	Cu	Fe	Zr
$Cu_{49.5}Fe_{49.5}Zr_1$	60 days	(γFe)/$Fe_{23}Zr_6$/(Cu)	7.3	92.7	0.0	6.0	73.5	20.5	93.6	6.4	0.0
$Cu_{47.5}Fe_{47.5}Zr_5$	60 days	(γFe)/$Fe_{23}Zr_6$/(Cu)	7.2	92.8	0.0	5.2	74.2	20.6	94.1	5.8	0.1
$Cu_5Fe_{85}Zr_{10}$	60 days	(γFe)/$Fe_{23}Zr_6$	5.1	94.9	0.0	3.3	76.0	20.7			
$Cu_{41}Fe_{41}Zr_{18}$	4 days	Fe_2Zr/$Fe_{23}Zr_6$/(Cu)	6.3	68.1	25.6	4.6	75.8	19.6	94.6	5.4	0.0
$Cu_{37}Fe_{37}Zr_{26}$	4 days	Fe_2Zr/Liquid/(Cu)	7.1	64.1	28.8	87.8	4.0	8.2	96.6	3.4	0.0
$Cu_{60}Fe_{10}Zr_{30}$	12 h	Fe_2Zr/Liquid/$Cu_{51}Zr_{14}$	14.0	54.0	32.0	58.5	6.0	35.5	78.3	1.0	20.7
$Cu_{30}Fe_{30}Zr_{40}$	21 days	Fe_2Zr/Liquid	11.2	56.4	32.4	29.3	14.1	56.6			
$Cu_{10}Fe_{50}Zr_{40}$	4 days	Fe_2Zr/Liquid	5.2	60.8	34.0	22.7	20.5	56.8			
$Cu_{27.5}Fe_{27.5}Zr_{45}$	21 days	Fe_2Zr/Liquid	11.1	56.5	32.4	29.8	13.5	56.7			
$Cu_{25}Fe_{25}Zr_{50}$	21 days	Fe_2Zr/Liquid	3.0	64.0	33.0	19.8	22.8	57.4			
$Cu_{10}Fe_{40}Zr_{50}$	4 days	Fe_2Zr/Liquid	2.7	63.2	34.1	13.3	20.9	65.8			
$Cu_5Fe_{45}Zr_{50}$	21 days	Fe_2Zr/Liquid	1.2	66.2	32.6	8.0	26.7	65.3			
$Cu_9Fe_9Zr_{82}$	21 days	(βZr)/Liquid	0.1	0.1	99.8	10.6	13.7	75.7			
$Cu_5Fe_{10}Zr_{85}$	4 days	(βZr)/Liquid	0.0	0.1	99.9	7.1	16.6	76.3			
$Cu_5Fe_5Zr_{90}$	4 days	(βZr)/Liquid	2.9	2.8	94.3	15.5	14.6	69.9			

Table 4 Equilibrium compositions of the Cu-Fe-Zr system at 1100 °C

Alloys, at.%	Annealing time	Phase equilibria Phase 1/Phase 2/Phase 3	Composition, at.%								
			Phase 1			Phase 2			Phase 3		
			Cu	Fe	Zr	Cu	Fe	Zr	Cu	Fe	Zr
$Cu_{49.5}Fe_{49.5}Zr_1$	2 days	(γFe)/Liquid	7.0	93.0	0.0	90.7	4.5	4.8			
$Cu_{48.5}Fe_{48.5}Zr_3$	4 days	(γFe)/Liquid	6.7	93.3	0.0	94.1	5	0.9			
$Cu_{47.5}Fe_{47.5}Zr_5$	4 days	(γFe)/Liquid	6.8	93.2	0.0	93.6	4.3	2.1			
$Cu_{46.5}Fe_{46.5}Zr_7$	4 days	(γFe)/$Fe_{23}Zr_6$/Liquid	6.5	93.3	0.2	7.4	72.4	20.2	92.4	5	2.6
$Cu_{45.5}Fe_{45.5}Zr_9$	4 days	(γFe)/$Fe_{23}Zr_6$/Liquid	6.7	93.3	0.0	7.6	72.6	19.8	90.5	4.9	4.6
$Cu_{45}Fe_{45}Zr_{10}$	4 days	(γFe)/$Fe_{23}Zr_6$/Liquid	7.4	92.6	0.0	7.1	72.0	20.9	90.8	5.2	4
$Cu_5Fe_{85}Zr_{10}$	60 days	(γFe)/$Fe_{23}Zr_6$	5.1	94.8	0.1	3.6	75.8	20.6			
$Cu_{43.5}Fe_{43.5}Zr_{13}$	4 days	Fe_2Zr/$Fe_{23}Zr_6$/Liquid	5	67.5	27.5	6.8	73.2	20.0	93.20	3.0	3.8
$Cu_{41}Fe_{41}Zr_{18}$	4 days	Fe_2Zr/$Fe_{23}Zr_6$/Liquid	5.3	67.6	27.1	6.3	73.7	20.0	92.0	3.1	4.9
$Cu_{38}Fe_{38}Zr_{24}$	1 day	Fe_2Zr/Liquid	13.6	55.7	30.7	71.0	8.1	20.9			
$Cu_{37}Fe_{37}Zr_{26}$	1 day	Fe_2Zr/Liquid	7	62.5	30.5	83.3	4.5	12.2			
$Cu_{30}Fe_{30}Zr_{40}$	12 h	Fe_2Zr/Liquid	9.9	57.6	32.5	68.1	6.6	25.3			
$Cu_{10}Fe_{50}Zr_{40}$	4 days	Fe_2Zr/Liquid	8.5	58.5	33	52.5	11.2	36.3			
$Cu_{25}Fe_{25}Zr_{50}$	1 day	Fe_2Zr/Liquid	9.1	57.8	33.1	41.4	11.6	47.0			
$Cu_{10}Fe_{40}Zr_{50}$	4 days	Fe_2Zr/Liquid	4.5	63.0	32.5	19.1	21.4	59.5			
$Cu_5Fe_{45}Zr_{50}$	4 days	Fe_2Zr/Liquid	3	65.8	31.2	12.3	24.1	63.6			
$Cu_9Fe_9Zr_{82}$	4 days	(βZr)/Liquid	0.3	0.1	99.6	12.2	9.4	78.4			
$Cu_{10}Fe_5Zr_{85}$	4 days	(βZr)/Liquid	0.4	0.1	99.5	15.3	6.3	78.4			
$Cu_5Fe_{10}Zr_{85}$	4 days	(βZr)/Liquid	0.1	0.1	99.8	9.0	11.5	79.5			

Table 5 Equilibrium compositions of the Cu-Fe-Zr system at 1200 °C

Alloys, at.%	Annealing time	Phase equilibria Phase 1/Phase 2/Phase 3	Composition, at.%								
			Phase 1			Phase 2			Phase 3		
			Cu	Fe	Zr	Cu	Fe	Zr	Cu	Fe	Zr
$Cu_{49.5}Fe_{49.5}Zr_1$	1 day	(γFe)/Liquid	8.4	91.6	0.0	95.9	4.1	0.0			
$Cu_{48.5}Fe_{48.5}Zr_3$	2 days	(γFe)/Liquid	8.0	92	0.0	95.0	5.0	0.0			

Table 5 continued

Alloys, at.%	Annealing time	Phase equilibria Phase 1/Phase 2/Phase 3	Composition, at.%								
			Phase 1			Phase 2			Phase 3		
			Cu	Fe	Zr	Cu	Fe	Zr	Cu	Fe	Zr
$Cu_{47.5}Fe_{47.5}Zr_5$	2 days	(γFe)/Liquid	7.7	92.3	0.0	96.8	3.2	0.0			
$Cu_{45}Fe_{45}Zr_{10}$	2 days	(γFe)/$Fe_{23}Zr_6$/Liquid	7.1	92.9	0.0	10.9	68.4	20.7	90.1	5.2	4.7
$Cu_{41}Fe_{41}Zr_{18}$	2 days	Fe_2Zr/$Fe_{23}Zr_6$/Liquid	5.2	68.5	26.3	7.1	72.5	20.4	92.8	3.3	3.9
$Cu_{38}Fe_{38}Zr_{24}$	2 days	Fe_2Zr/$Fe_{23}Zr_6$/Liquid	6.9	64.7	28.4	9.0	70.9	20.1	89.3	2.7	8.0
$Cu_{30}Fe_{30}Zr_{40}$	6 h	Fe_2Zr/Liquid	10.1	54.6	35.3	69.7	6	24.3			
$Cu_{20}Fe_{40}Zr_{40}$	2 days	Fe_2Zr/Liquid	10.5	57.6	31.9	76.9	7.9	15.2			
$Cu_{10}Fe_{50}Zr_{40}$	2 days	Fe_2Zr/Liquid	7.7	59.2	33.1	43.6	12.7	43.7			
$Cu_{27.5}Fe_{27.5}Zr_{45}$	2 days	Fe_2Zr/Liquid	9.9	55.0	35.1	72.6	7.2	20.2			
$Cu_{25}Fe_{25}Zr_{50}$	1 h	Fe_2Zr/Liquid	5.7	62.2	32.1	23.6	19.8	56.6			
$Cu_{10}Fe_{40}Zr_{50}$	2 days	Fe_2Zr/Liquid	3.2	64.1	32.7	19.8	17.9	62.3			
$Cu_5Fe_{45}Zr_{50}$	2 days	Fe_2Zr/Liquid	1.3	65.5	33.2	8.9	25.5	65.6			
$Cu_9Fe_9Zr_{82}$	2 days	(βZr)/Liquid	0.2	0.0	99.8	11.7	9.5	78.8			
$Cu_5Fe_{10}Zr_{85}$	2 days	(βZr)/Liquid	0.1	0.0	99.9	7.8	12.1	80.1			
$Cu_5Fe_5Zr_{90}$	2 days	(βZr)/Liquid	0.2	0.0	99.8	6.8	8.8	84.4			

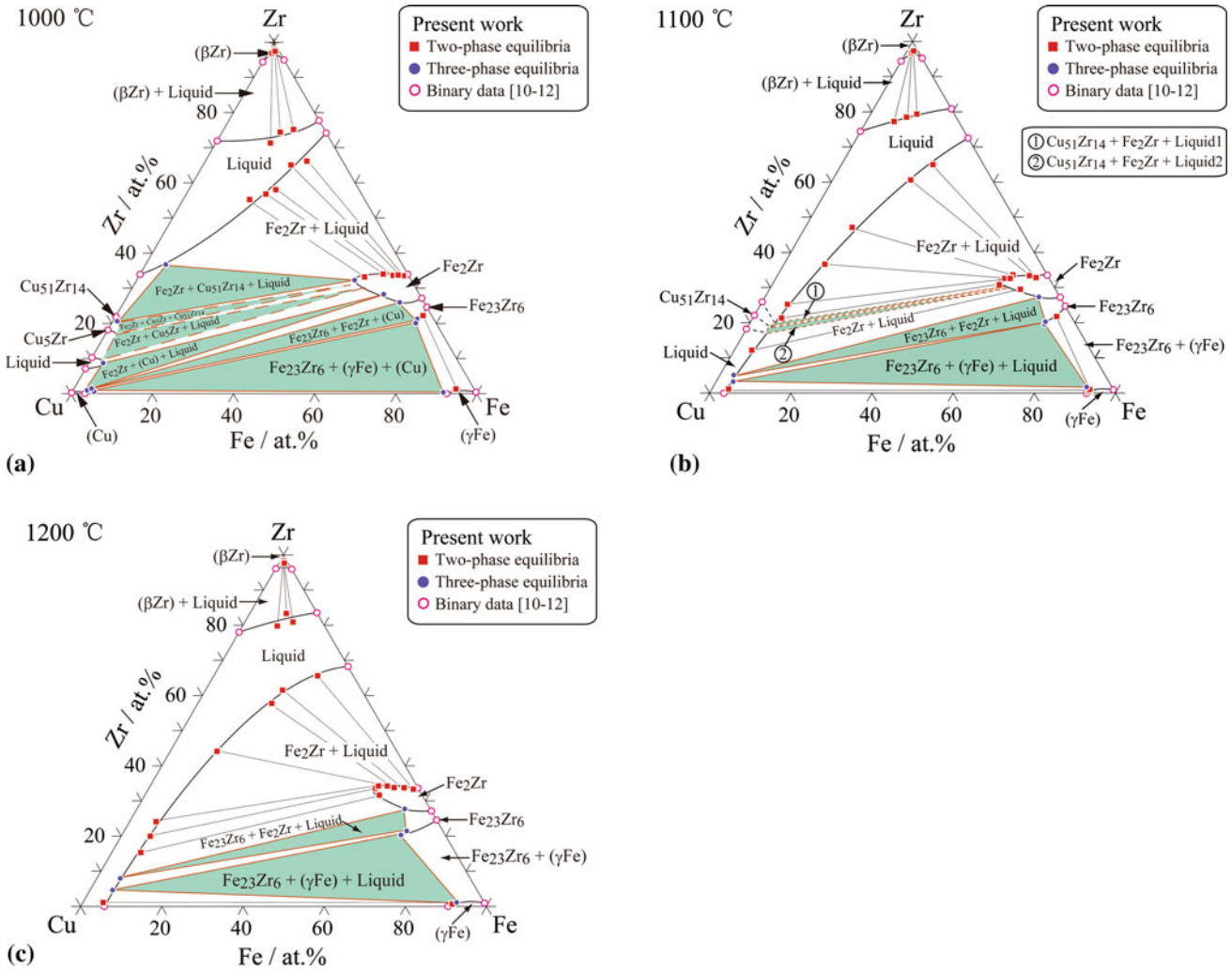

Fig. 5 Experimentally determined isothermal sections of the Cu-Fe-Zr system at: (a) 1000 °C, (b) 1100 °C and (c) 1200 °C

4. Conclusions

The isothermal sections of the Cu-Fe-Zr ternary system at 1000, 1100 and 1200 °C were experimentally determined by the means of EPMA and XRD. The area of liquid phase increases at the temperature ranging from 1000 to 1200 °C.

Acknowledgments

This work was supported by the National Natural Science Foundation of China (Grant Nos. 51031003 and 51201145) and the Ministry of Science and Technology of China (Grant No. 2009DFA52170). The support from the National Key Basic Research Program of China (973 Program, 2012CB825700) is also acknowledged.

References

1. M.E. McHenry, M.A. Willard, and D.E. Laughlin, Amorphous and Nanocrystalline Materials for Applications as Soft Magnets, *Prog. Mater. Sci.*, 1999, **44**, p 291-433
2. W.H. Wang, C. Dong, and C.H. Shek, Bulk Metallic Glasses, *Mater. Sci. Eng. R*, 2004, **44**, p 45-89
3. J. Tan, Y. Zhang, B.A. Sun, M. Stoica, C.J. Li, K.K. Song, U. Kühn, F.S. Pan, and J. Eckert, Correlation Between Internal States and Plasticity in Bulk Metallic Glass, *Appl. Phys. Lett.*, 2011, **98**, p 151906-1-3
4. M.G. Chen, A Brief Overview of Bulk Metallic Glasses, *NPG Asia Mater.*, 2011, **3**, p 82-90
5. J. He, H.Q. Li, B.J. Yang, J.Z. Zhao, H.F. Zhang, and Z.Q. Hu, Liquid Phase Separation and Microstructure Characterization in a Designed Al-Based Amorphous Matrix Composite with Spherical Crystalline Particles, *J. Alloy. Compd.*, 2010, **489**, p 535-540
6. H.J. Chang, W. Yook, E.S. Park, J.S. Kyeong, and D.H. Kim, Synthesis of Metallic Glass Composites Using Phase Separation Phenomena, *Acta Mater.*, 2010, **58**, p 2483-2491
7. Y. Yu, Y. Takaku, M. Nagasako, C.P. Wang, X.J. Liu, R. Kainuma, and K. Ishida, Liquid-Immiscibility-Induced Formation of Micron-Scale Crystalline/Amorphous Composite Powder, *Intermetallics*, 2012, **25**, p 95-100
8. B.R. Rao, A.K. Shan, M. Srinivas, J. Bhatt, A.S. Gandhi, and B.S. Murty, On Prediction of Amorphous Phase Forming Compositions in the Iron-Rich Fe-Zr-B Ternary System and Their Synthesis, *Metall. Mater. Trans. A*, 2011, **42A**, p 3913-3920
9. A.R. Miedema, P.F. de Châtel, and F.R. de Boer, Cohesion in Alloys-Fundamentals of a Semi-Empirical Model, *Physica B*, 1980, **100**, p 1-28
10. L.J. Swartzendruber, Cu-Fe (Copper-Iron), *Phase Diagrams for Binary Alloys*, 2nd ed., H. Okamoto, Ed., ASM International, Materials Park, 2010, p 308
11. H. Okamoto, Cu-Zr (Copper-Zirconium), *J. Phase Equilib. Diffus.*, 2008, **29**(2), p 204
12. H. Okamoto, Fe-Zr (Iron-Zirconium), *J. Phase Equilib. Diffus.*, 2006, **27**(5), p 543-544
13. I.K. Suh, H. Ohta, and Y. Waseda, High-Temperature Expansion of Six Metallic Elements Measured by Dilatation Method and X-Ray Diffraction, *J. Mater. Sci.*, 1988, **23**, p 757-760
14. D.R. Wilburn and W.A. Bassett, Hydrostatic Compression of Iron and Related Compounds: An Overview, *Am. Mineral.*, 1978, **63**, p 591-596
15. J. Haglund, F. Fernandez-Guillermet, F.G. Grimvall, and M. Korling, Theory of Bonding in Transition-Metal Carbides and Nitrides, *Phys. Rev. B*, 1993, **48**, p 11685-11691
16. P. Forey, J.L. Glimois, J.L. Feron, G. Develey, and C. Becle, Preparation, identification et structure cristalline de Cu_5Zr, *Comptes Rendus Hebdomadaires des Séances de l'Académie des Sciences C*, 1980, **291**, p 177-178
17. L. Bsenko, Crystallographic Data for Intermediate Phases in the Copper-Zirconium and Copper-Hafnium Systems, *J. Less-Common Met.*, 1975, **40**, p 365-366
18. E.M. Carvalho and I.R. Harris, Constitutional and Structural Studies of the Intermetallic Phase ZrCu, *J. Mater. Sci.*, 1980, **15**, p 1224-1230
19. M.V. Nevitt and J.W. Downey, A Family of Intermediate Phases Having the Si_2Mo-Type Structure, *Trans. Metall. Soc. AIME*, 1962, **224**, p 195-196
20. N.V. German, A.A. Bakanova, L.A. Tarasova, and Yu.N. Sumulov, Phase Transition of Titanium and Zirconium in Shock Waves, *Solid State Phys.*, 1970, **12**, p 637-639
21. B. Olinger and J.C. Jamieson, Zirconium: Phases and Compressibility to 120 Kilobars, *High Temp. High Press.*, 1973, **5**, p 123-131
22. P.I. Kripyakevich, V.S. Protasov, and E.E. Cherkashin, Crystal Structure of the Compound $ZrFe_3$, *Zh. Neorg. Khim.*, 1965, **10**(1), p 151-152
23. A. Israel, I. Jacob, J.L. Soubeyroux, D. Fruchart, H. Pinto, and M. Melamud, Neutron Diffraction Study of Atomic Bonding in the Hydrogen-Absorbing $Zr(Al_xFe_{1-x})_2$ System, *J. Alloy. Compd.*, 1997, **253**, p 265-267
24. E.E. Havinga, H. Damsma, and P. Hokkeling, Compounds and Pseudo-Binary Alloys with the $CuAl_2$(C16)-Type Structure. I. Preparation and X-Ray Results, *J. Less-Common Met.*, 1972, **27**, p 169-186
25. K.H.J. Buschow, I. Vincze, and F. van der Wonde, Crystallization of Amorphous Zr-Rich Alloys, *J. Non-Cryst. Solids*, 1983, **54**, p 101
26. F. Stein, G. Sauthoff, and M. Palm, Experimental Determination of Intermetallic Phases, Phase Equilibria, and Invariant Reaction Temperatures in the Fe-Zr System, *J. Phase Equilib. Diffus.*, 2002, **23**(6), p 480-494